Carbon and Oxygen Isotopic Fractionation in the products of low-temperature VUV photodissociation of Carbon Monoxide

Subrata Chakraborty[1], Bruce Rude[2], Musahid Ahmed[2], and Mark H. Thiemens[1]

[1]Department of Chemistry and Biochemistry, University of California, San Diego, La Jolla, California 92093-0356, [2] Chemical Sciences Division, Lawrence Berkeley National Laboratory, 1 Cyclotron Road, Berkeley, CA 94720.

Abstract

The carbon and oxygen isotope fractionations occurring during photodissociation of carbon monoxide (CO) by vacuum ultraviolet photons (91 to 107 nm) at 80K were measured and the isotopic fractionations due to direct and indirect predissociation processes individually quantified. The isotopic fractionations depend on the photodissociation wavelength. Slope values ($\delta^{17}O/\ \delta^{18}O$) in oxygen three-isotope space range from 0.75 to 1.1. The isotopic composition of the products depends on the dissociation dynamics at the upper electronic state (perturbation and coupling associated with that state), which in turn modulates the isotope effect (in this case an enrichment of minor isotopes) inside the gas column due to the saturation of major isotopologue (isotope self-shielding). An explanation in terms of isotope self-shielding would require a quantum yield of one for photodissociation of all isotopologues which is not consistent with the data.

1. Introduction

CO is the second most abundant molecule in the interstellar medium after hydrogen. In the solar nebula, it is the most abundant oxygen and carbon carrying primordial molecule. The conventional self-shielding model [1, 2] can enrich oxygen equally in ^{17}O and ^{18}O and create a slope 1 array in oxygen three-isotope plot [3] as measured in meteorite silicates. The implication is that the oxygen locked in silicates (except in case of early refractory condensates) were all processed through CO photodissociation in solar nebula or in parent molecular cloud [4].

1.1 Photochemistry and Isotopic Fractionation

Carbon monoxide (CO) absorbs photons in several discrete actinic bands in the vacuum ultraviolet (VUV) region where the observed emission spectra indicate that the bands are all predissociative [5-7], i.e., the excited molecules dissociate indirectly following the transition from a bound to a repulsive surface. Here photo-excitation occurs to nominally bound ro-vibrational levels of an electronically excited state that has perturbative interaction with the continuum or the bound state of another electronic state. Direct predissociation occurs through various types of interaction between the bound state and the continuum, e.g., spin-orbit, hyperfine, electrostatic, rotational and gyroscopic. The dissociation cross-section is governed by Fermi's Golden Rule and depends on the coupling between the bound excited state and dissociative states [8-10]. Phase differences between the bound and continuum vibrational wave functions influence the line-width for dissociation based on the location of the crossing points of the two relevant electronic surfaces. The relative dissociation probability of isotopically substituted species differs due to changes in transition probability to the upper electronic states. Indirect predissociation occurs where the predissociated rotational-vibrational level is perturbed by another rotational-vibrational level

that is directly predissociated by a third (unbound) state [11, 12]. The accidentally predissociated level has an admixture of the perturbing wave functions, acquiring a portion of the perturbed state characteristics. The line widths are highly sensitive to isotopic substitution [6, 10, 13]. Because of the complexities associated with predissociation, a generalized formulation [14, 15] to calculate the isotopic effect is not possible in contrast to the case of direct photodissociation [16] and must be calculated separately for individual molecules.

Using the Advanced Light Source (ALS) synchrotron, the isotopic fractionation factors for different predissociative molecules (e.g., CO, N_2, SO_2, H_2S, OCS) [11, 17-21] have been determined. In case of N_2, all spectroscopic parameters are known [22], but experimental studies of photodissociation show that the measured fractionations differ significantly from the computed ones [20, 23]. This underscores the need for experimental measurements of wavelength specific isotopic fractionations. Our recent N_2 photodissociation experiments at low temperature (80 K) reveal that the fractionations are temperature sensitive [21] and indicate that the ro-vibrational levels play a significant role during the perturbation process. Rotational levels are temperature dependent and thus changes in temperature influences the perturbation geometry and in turn the isotopic fractionation. However, unlike N_2, a complete set of spectroscopic data does not exist for CO which makes the interpretation difficult [24-29].

1.2 Rationale Behind the Study

The fractionation factors of different molecules in dissociative processes are required to interpret the isotopic record in environments relevant to geochemistry, cosmochemistry and atmospheric and planetary sciences. As mentioned, the pre-dissociative processes are temperature sensitive and thus for application purpose the fractionation factors for relevant temperatures are needed. Our previous CO photodissociation experiments were performed at ambient (300 K) and dry ice (200 K) temperatures. Moreover, only the isotopes of oxygen were measured [11, 17, 18]. Here we report results of CO photodissociation experiments at a very low-temperature of 80 K to determine both the associated carbon and oxygen isotopic fractionations of the products which may provide new insight into the predissociation process for CO [21].

This data set is meant to interpret astrophysical observations and meteorite data. Therefore, we need to design the experiments to represent the astrophysical conditions to some degree. In many astrophysical environments, CO molecules are present and their photodissociation takes place in the relatively cold region where the concentrations of H_2 and H are larger by about 10^4 than the concentration of CO. Though in the present experiments the temperatures are in the correct range, performing the experiments with nebula-like H_2/CO ratio was not feasible. We used a lower ratio of H_2/CO (1:1) to monitor any possible additional effect on O-isotope fractionation by comparing the results with the case where no H_2 was used [11, 17].

2. Isotope Self-Shielding

When light passes through a column of gas and dissociates the molecules by line absorption, differential absorption of light occurs for the individual isotopologues which are proportional to their number densities or isotopic abundances. As a result, when the band heads of the isotopologues are sufficiently separated, the spectral line corresponding to the major species may be totally absorbed (saturate) but the lines corresponding to the minor species may be still present and selective photodissociation of minor species could occur within the subsequent part of the gas column [18]. This process is termed isotope self-shielding (or isotope selective photodissociation further along the path). Several absorption bands of CO satisfy these conditions for isotope selective photodissociation

(described in more detail in the following section). In other words, when the spectral line corresponding to the major isotopologue $^{12}C^{16}O$ saturates, the lines corresponding to the minor isotopologues (e.g., $^{12}C^{17}O$, $^{12}C^{18}O$ and $^{13}C^{16}O$) are still available, and as a consequence preferential production of ^{17}O and ^{18}O atomic species occurs in the wavelength region of relevance [5, 30, 31]. This process also assumes that absorption of each photon produces an immediate dissociation. This work tests the basic assumption that no isotopic selectivity occurs in the dissociation process as assumed in the self-shielding model.

3. The Position of the CO Absorption Bands within a Synchrotron Band

There are approximately 41 strong absorption bands [5, 30, 32] in the wavelength region 90 to 108 nm for CO. However, all absorption bands are not equally effective for dissociating CO. The absorption band possessing the largest oscillator strength produces the maximum dissociation [5, 32]. The FWHM of the synchrotron beam is 2.2 nm and within the umbrella of a synchrotron band, several CO absorption bands are present [8, 18, 32]. To cover the entire range of CO photodissociation bands, a total of six synchrotron bands are used in the present experiment whose beams are centered at 91, 92, 94.12, 97.03, 105.17, 107.61 nm. A detailed description of the CO absorption bands and the synchrotron bands is given in our previous publication [11]. The characteristics of the CO absorption bands are not same [8, 32-39] and each individual one needs to be analyzed carefully.

Self-shielding is only possible for a particular CO absorption band when the band heads of the isotopologues are adequately separate. The separations are quite large (49.26 and 51.18 cm^{-1}) between the band heads of $C^{16}O$ and $C^{18}O$ isotopologues for the 105.17 and 106.31 nm bands [40] respectively. Consequently, both these bands may produce self-shielding. The band heads of $^{12}C^{16}O$, $^{13}C^{16}O$, $^{12}C^{17}O$, and $^{12}C^{18}O$ isotopologues for the 107.61 nm band are very closely spaced (within 1 cm^{-1}) [18, 41] and are not resolvable for $^{13}C^{16}O$, $^{12}C^{17}O$, and $^{12}C^{18}O$, which render the 107.61 nm band a shielding band for $^{12}C^{16}O$. Table 2 and Figure 4 of our earlier paper [11] summarizes the description presented above.

4. Methodology

4.1. Experimental Details

VUV photolysis of CO was carried out in a differentially pumped reaction chamber [20] at temperatures close to 80K (through liquid nitrogen (LN_2) cooling) as shown schematically in Figure 1. A steady flow (0.1 sccm) of high purity premixed gas ($CO:H_2 = 50:50$) was established in the reaction chamber at CO partial pressure of 100 mtorr (a few experiments were performed with 20 and 50 mtorr of CO partial pressures). Photolysis of this gas mixture was carried out at six different synchrotron bands (FWHM > 2 nm, Advanced Light Source, LBNL, Berkeley, CA) between 91 and 107 nm, as mentioned above, covering all the 41 CO absorption bands for about 8 hours each. During the experimental runs, photolysis products (CO_2 and possibly H_2O) were trapped in the inner wall of the cold chamber. To avoid any loss of the products through the outflowing of gas, three spiral traps cooled with LN_2 were placed in line. At the end of each run, the reaction chamber temperature was elevated slightly above the room temperature using a heat gun and the samples were collected in the traps kept at LN_2 temperature. The first two traps were then thawed and their contents collected in the third trap. Subsequently, this trap was submerged inside a -90 C ethanol slush bath and the products CO_2 and H_2O were cryogenically separated and stored in pre-evacuated metal sample tubes fitted with a Swagelok valve and returned to UC, San Diego for isotopic analysis.

An experiment was performed at 300 mtorr for 300 min without any synchrotron photons (blank experiment) and < 0.2 μmoles of condensable gases were collected in the LN_2 traps. Based on the cryogenic property of this collected gas, we conclude that the major

part of this blank is water vapor. The CO_2 produced in all the experiments were cryogenically cleaned (from potential water vapor) before analysis as described above.

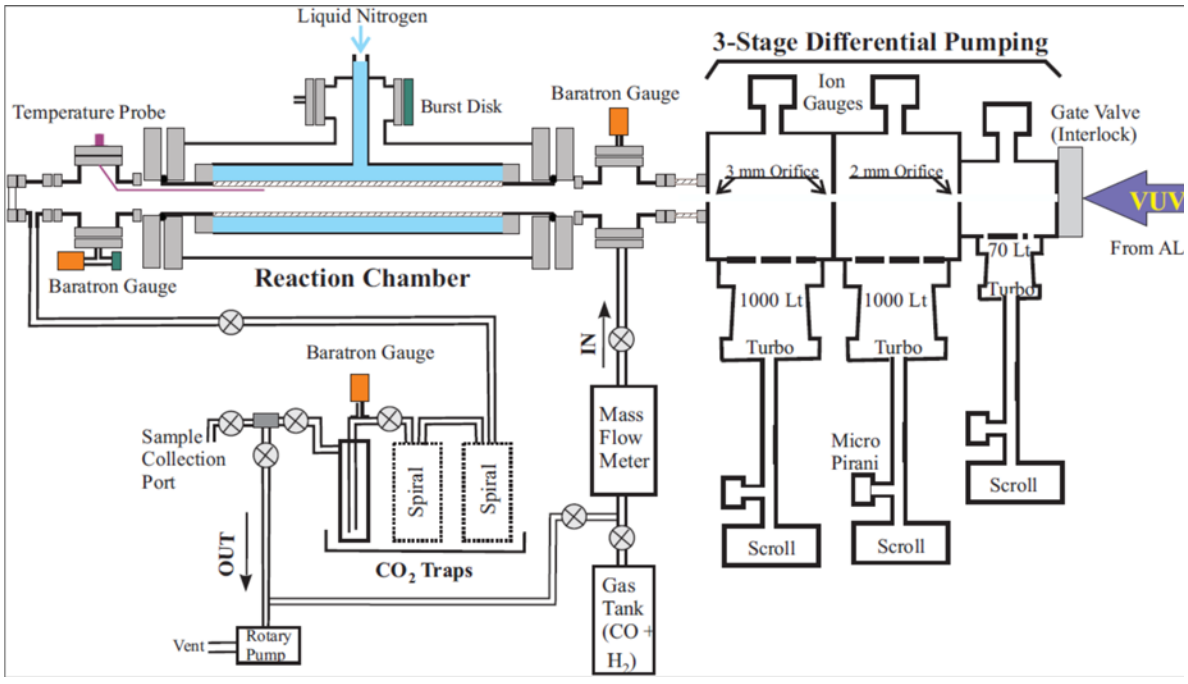

Figure 1. *Schematic of the experimental set-up used in this experiment. The window-less chamber was coupled to the synchrotron beamline through 3-stage differential pumping sector.*

4.2. Expression of Isotope Ratios

The sample isotopic ratios are expressed in the usual δ-notation defined below (denoting fractional deviation from a chosen standard isotope ratio) for an element X with two isotopes a (major) and b (minor):

$$\delta^{b}X = [({}^{b}X/{}^{a}X)_{sample}/({}^{b}X/{}^{a}X)_{std} - 1] \qquad (1)$$

or in logarithmic form (for large δ-values, due to non-linearity),

$$\delta'^{b}X = \ln[1 + \delta^{b}X/10^{3}) \qquad (2)$$

and expressed in per mil (‰). Following this definition, the carbon isotope ratio $^{13}C/^{12}C$ is expressed as $\delta^{13}C$ and two oxygen isotope ratios are expressed as $\delta^{17}O$ and $\delta^{18}O$. The δ′ values are given relative to the starting composition.

4.3. Determination of Carbon Isotopic Composition

For oxygen ($\delta^{18}O$) and carbon ($\delta^{13}C$) isotopic analysis, the ratios of CO_2 isotopologues 45/44 and 46/44 are measured in an isotope ratio mass spectrometer (IRMS). The isotopologue of mass 45 could be formed by two isotopic variants, i.e., $^{12}C^{17}O^{16}O$ and $^{13}C^{16}O^{16}O$. In a normal fractionation process, when oxygen isotopes are mass dependently fractionated (e.g., $\delta^{17}O \sim 0.5 \times \delta^{18}O$), $\delta^{17}O$ values are obtained from $\delta^{18}O$ values and used to determine $\delta^{13}C$ [42]. However, it is known from our previous results [11, 17] that the oxygen isotopic composition of the product CO_2 from CO photodissociation does not follow the mass-dependent rule (i.e., $\delta^{17}O \neq 0.5 \times \delta^{18}O$), and we need to use a different procedure to obtain the three delta values. Firstly, the isotopologue ratios 45/44 and 46/44 of product CO_2 samples were measured on aliquots of each sample (46/44 ratio yielded the $\delta^{18}O$ value of the sample). In the next step, another aliquot

of the product CO_2 was equilibrated separately with CuO inside a Ni-vessel at 900 °C for 2 hours to erase any mass-independent oxygen isotopic signature and the equilibrated CO_2 was re-measured for the same isotopologue ratios (CO_2 yield of this equilibration process is 100 %). The second set of ratio measurements yields the $\delta^{13}C$ value of the sample assuming mass dependence of ^{17}O and ^{18}O composition. Substituting this value back into the ratios of the first set of measurements yields the $\delta^{17}O$ value of the CO_2 sample.

4.4. Self-shielding Model Calculation

The process of isotopic self-shielding (or isotope selective photodissociation) is expressed through:

$$I = Io\ exp(-\sigma cl) \qquad (3)$$

where: I = photon flux at length l *(at the end of the chamber)*, I_o = initial photon flux at l = *0 (beginning of the chamber, at the photon entrance slit)*, c = concentration (molecules per cm^3), l = optical path length (cm) taken as the length of the chamber, σ = cross-section (cm^2). The concentration of the gas was determined using the ideal gas law by knowing the pressure of the gas (measured by a capacitance manometer) and chamber volume (determined during fabrication of the chamber). For the ALS synchrotron beamline 9.0.2 (Chemical Dynamics Beamline), the wavelength dependent photon flux follows a nearly Gaussian profile (with a tail on the right) with FWHM = 0.25 eV. The photodissociation experiments are performed centering this Gaussian-shaped beam at six different wavelengths mentioned above where several CO absorption bands fall under the umbrella of each synchrotron band. A MATLAB code was previously written to calculate the isotope self-shielding of N_2 [20]. We have modified the same code to track the concentrations of all the atomic species (i.e., ^{12}C, ^{13}C, ^{16}O, ^{17}O and ^{18}O) that are generated along the length of the chamber as per the following equation,

$$N^x = \int_{\lambda 1}^{\lambda 2} I_0(1 - e^{-\sigma_\lambda^x c^x l})\ d\lambda \qquad (4)$$

where: N^x is the number of atomic species of mass x, σ_λ^x is the cross-section of an isotope (x) at a wavelength λ. λ_1 *and* λ_2 *are* the lower and upper limits of the synchrotron beam width (FWHM), c^x is the concentration of the CO isotopologue (x) at the wavelength λ. The initial photon flux (*Io*) is not the same for all the absorption bands under one synchrotron band as the synchrotron band has a near Gaussian shape [18]. A fit function: $I_0 = y_0 + a/(1 + \left(\frac{\lambda - \lambda_0}{b}\right)^2)$,

where: a *= 286.1213,* b*=1777.696,* y_0*= -13.6190,* λ_0*= synchrotron beam center*

was utilized to precisely define the synchrotron beam profile centered at the wavelength of interest (λ_0). Under each synchrotron beam profile, *Io* value corresponding to each CO absorption band is assigned in the code. The code then determines the *I*-values for all the isotopologue specific bands utilizing equation (4) and knowing the required parameters, e.g., c^x and l as used for the experiment and σ_λ^x-values from the literature [27] and personal communication (Prof. Michele Eidelsberg for ^{12}CO, ^{13}CO, $C^{18}O$ with the wavelength range of 92 through 97 nm). The code calculates the number density of each isotope of C and O at the end of the exposure time. It then computes the isotopic ratios and hence the δ-values. Table 1 shows the parameter used to run the model code. The measured molecular constant data to compute the absorption cross-section for one of the rare isotopologues, $C^{17}O$ is not available at present [43] and we used values based on the literature data [2, 5, 25-27, 33, 34, 40, 43]. The MATLAB code and the cross-sectional data set are provided in the online database [44]. The code used those data sets of σ-values and computed the isotopic composition of oxygen and carbon in the product pool with the assumption that the quantum yield is unity for all the bands upon dissociation. The code then computes the

carbon and oxygen isotopic compositions of CO_2 species (i.e., a combination of three isotopes of oxygen and two isotopes of carbon) and computes the δ′-values using equations 1 and 2. The model code does not compute the amount of CO_2 produced, neither it incorporates the isotopic fractionation associated with the reaction forming CO_2. The uncertainty in the cross-section values range between 10 to 15 % and produce a 400 to 600 ‰ uncertainty in the delta values.

Table 1. Summary of the parameters used in the MATLAB model code to calculate the isotope effect due to self-shielding

Parameters	Values
Synchrotron Beam Centers (an input parameter)	91, 92, 94.12, 97.03, 105.17, 107.61 nm
Synchrotron Photon Flux	5 x 10^{14} Photons/ sec
Column Density (= concentration x length, an input parameter)	2 x 10^{17} molecules/ cm^2 (used for Figures 1 and 2)
Cross-section (σ)	Used the wavelength vs. cross-section data file as referred

5. Results

5.1. Experimental Data

Table 2. Summary of the experimental results. The delta values are relative to the starting CO composition ($\delta^{17}O$ = 25.5, $\delta^{18}O$ = 51 ‰ relative to SMOW; $\delta^{13}C$ = -26.5 ‰ rel. to VPDB. 2 to 10 μmole of CO_2 forms from about 1.8 moles of CO (flow rate was measured as 0.1 sccm). The CO_2 yield¶ variation shown in the table are mainly due to variation in CO absorption cross-section.

Expt No	CO-Partial Pressure (mTorr)	Wave Length (nm)	Energy (eV)	Exp Time (min)	Amount¶ (μmole)	Product CO_2 Composition¶¶ (‰)			Atomic Oxygen Composition (‰)	
						$\delta'^{17}O$ (‰)	$\delta'^{18}O$ (‰)	$\delta'^{13}C$ (‰)	$\delta'^{17}O$ (‰)	$\delta'^{18}O$ (‰)
ALS-15-07C	100	91.37	13.57	450	5.4	644	649	711	1215	1178
ALS-15-05C	100	92.6	13.39	440	10.1	1797	1975	842	3520	3830
ALS-15-04C	100	94.12	13.18	450	9.0	21623	2416	1132	4251	4711
ALS-14-10C	100	97.03	12.78	430	7.0	665	770	363	1257	1419
ALS-14-11C	100	105.17	11.79	462	6.7	967	847	103	1859	1574
ALS-15-06C	100	105.17	11.79	490	10.6	1181	992	149	2288	1863
ALS-15-09C	50	105.17	11.79	460	5.1	1208	960	629	2343	1799
ALS-15-10C	27.5	105.17	11.79	340	3.3	1158	1046	409	2242	1971
ALS-16-03C	20	105.17	11.79	465	2.8	1219	1345	384	2365	2571
ALS-15-08C	100	107.61	11.52	453	1.9	1054	1137	839	2034	2153
ALS-16-01C	50	107.61	11.52	420	3.5	1558	1610	372	3042	3099
ALS-16-02C	20	107.61	11.52	420	2.4	1405	1448	435	2737	2776

¶*Each CO after dissociation gives one C and one O atom and the product O combines with CO (initial) to produce CO_2. Therefore, the δ'-values of CO_2 is about ½ of that O. The yield of CO_2 or rate of production depends on the pressure of the initial CO, duration of photolysis, and the CO absorption cross-section at a particular wavelength.*

¶¶*Uncertainties in amount measurement are ± 0.2 μmoles and the external reproducibility (from start to finish) for all the isotope values are ± 50 ‰ based on the present and past experiments [11, 17, 18].*

The measured $\delta'^{13}C$, $\delta'^{17}O$ and $\delta'^{18}O$ values of the product CO_2 are shown in Table 2 in logarithmic form. The calculated values of atomic oxygen from CO dissociation are also shown in Table 2 and Figure 2a and 2b. Considering that CO_2 has formed from CO + O reaction and knowing the isotopic composition of initial CO and measured composition of CO_2 the isotopic composition of atomic oxygen can be determined by isotope mass balance (neglecting any fractionation in the reaction of O + CO). A Mass-independent oxygen isotopic effect (slope = 0.84) is known to occur in the CO + O recombination reaction [45]. The maximum magnitude of this effect in $\delta^{18}O$ was ~ 40 ‰, which is significant, but much less than the effects measured here (the effect of the recombination reaction is about the size of the symbols and cannot be reflected in the Figures). The inclusion of this fractionation has almost no effect on the slope values because the slope value (0.84) is very close to the values reported here. Figure 2 (a and b) depicts carbon and oxygen isotopic enrichment profiles (with respect to the initial (IN) composition, $\delta^{17}O$ = 25.5; $\delta^{18}O$ = 51 ‰ relative to SMOW [17]), respectively, of the product CO_2 showing an enrichment peak at 94 nm (with values of $\delta'^{18}O$ = 2415.5, $\delta'^{13}O$ = 1131.8 ‰). The oxygen isotopic distribution in three isotope space is shown in Figure 3. The isotopic compositions of atomic oxygen are significantly different and relatively enriched compared to that reported earlier [17] using the same wavelengths at ambient temperature (300 K). The reported slope ($\delta'^{17}O$/ $\delta'^{18}O$) values for 105 and 107 nm at ~300 K was 1.3 (shown in Figure 3 in greyscale). That reduced to 1.2 at 200 K (not shown in Figure 3); at 80 K the slope value reduced further to ~1.1 for 105 nm, and 0.95 for 107 nm. A slight pressure dependency is also noticed in the values (Table 2). The slopes at other wavelengths were measured within the range of 0.9 and 1.0. These values are mostly consistent with those previously measured at 300 K.

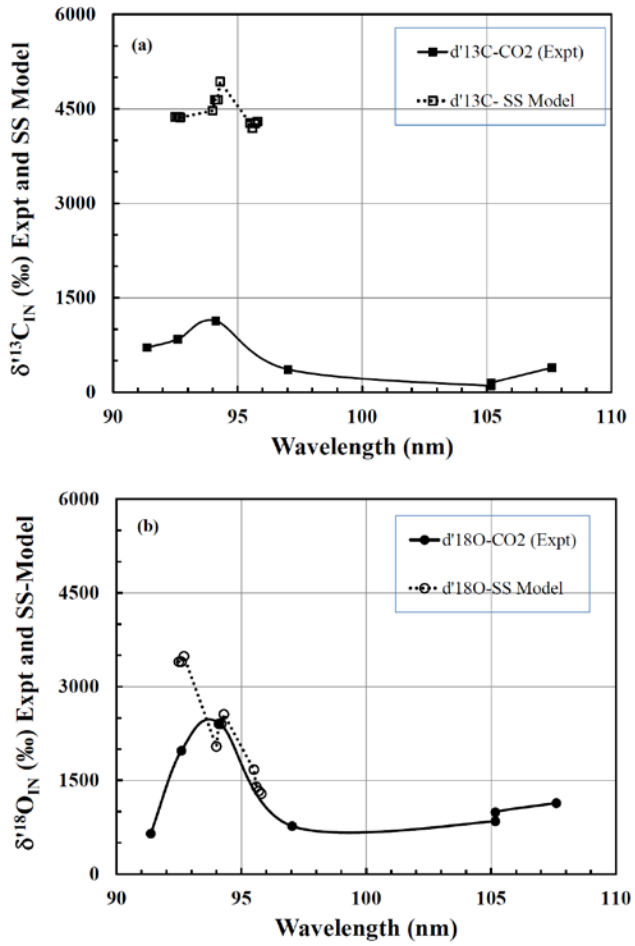

Figure 2. *Wavelength dependent isotopic composition ($\delta'^{13}C$ (a), $\delta'^{18}O$ (b)) variation in CO photodissociation product CO_2. Self-shielding based model computed data are shown through open symbols and dotted lines and they differ significantly from the experimental values (closed symbols) for a fixed column density. The δ'-values are relative to the initial CO composition denoted by subscript IN.*

5.2. Results from the self-shielding model

The wavelength dependency of isotopic fractionation from the self-shielding model calculations (for $\delta'^{18}O$ and $\delta'^{13}C$) are shown in Figures 2 (a and b) along with the experimental data. The range of calculated $\delta'^{18}O$ values are close to the measured range but the structure of wavelength dependence is quite different in the computed profile (Figure a, b). The computed $\delta'^{13}C$ values are about 4 to 5 times more enriched than the measured composition.

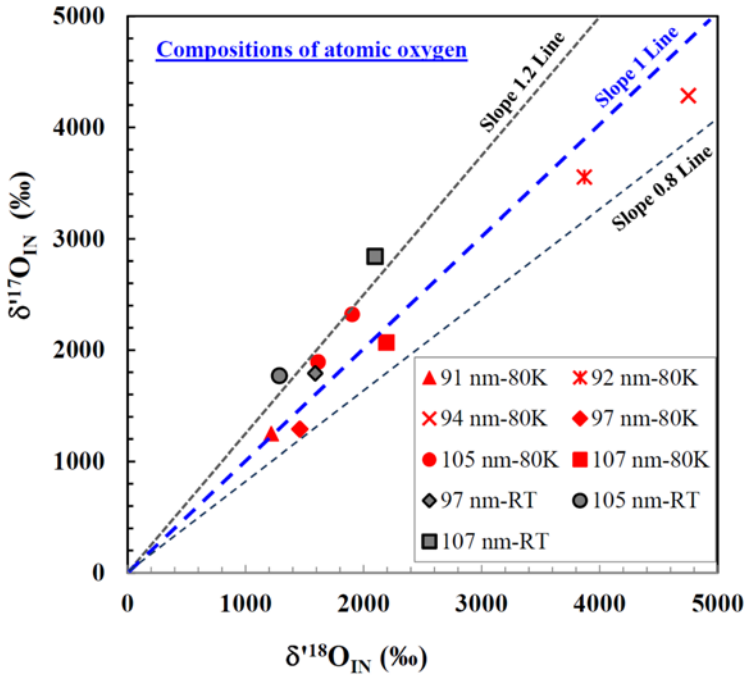

Figure 3. *Oxygen three-isotope plot showing the oxygen isotopic distribution in the product CO_2 (in terms of atomic O, relative to Initial (IN) CO composition). Varied range of slope ($\delta'^{17}O/\ \delta'^{18}O$) values are measured. The previous ambient temperature data are shown in grey. The slope (0.8, 1.0 and 1.2) lines are drawn for reference (and not data fits).*

6. Discussion

6.1. Oxygen isotopic fractionations

The observed wavelength specific isotopic composition of product CO_2 (shown in Figure 3 as atomic oxygen composition) indicates that all accessible excited electronic states do not dissociate in the same fashion. Some are more pre-dissociative and have different isotopic compositions. It seems that different excited electronic states accessed by VUV photons follow different dissociation dynamics based on the associated potential energy surfaces and local perturbations. With the lowering of temperature, upper rotational states are less populated and the absorption band structure changes significantly which alters the interaction between the overlapping states in the predissociation pathway [46], ultimately perturbing the overlapping wave functions. The wavelength dependent profiles of the degree of mass-independence, i.e., $\Delta'^{17}O$ (= $\delta'^{17}O$ – 0.515 x $\delta'^{18}O$) at three different temperatures (80, 200 and 300K) are different from each other (Figure 4). If the value of absorption cross-sections of the isotopologues were only affected by temperature, the profiles would have followed each other (the model code yields such behavior, though not shown here). Therefore, temperature affects the dissociation dynamics.

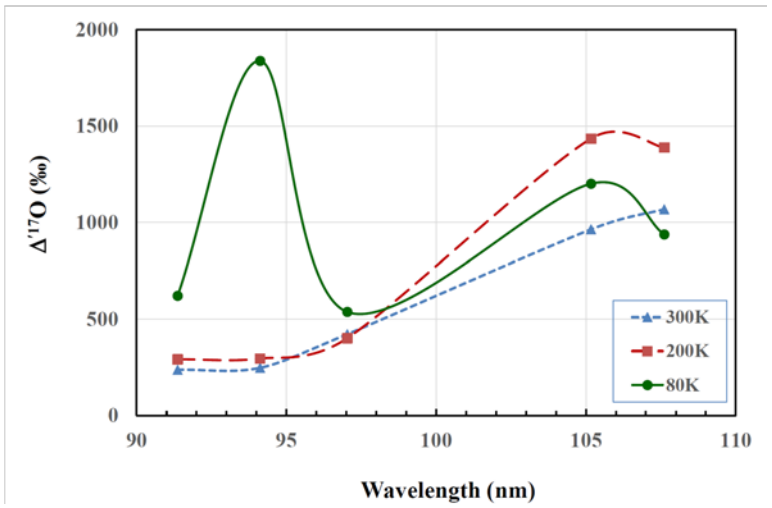

Figure 4. *Wavelength dependent $\Delta'^{17}O$ (= $\delta'^{17}O$ – 0.515 x $\delta'^{18}O$) values at three different temperatures: 80K (present experiment), 200 and 300K (from previous experiments) and, at CO partial pressure of 100 mtorr (when data from 100 mtorr CO pressure were not available for 200 K and 300K, δ-values from experiments nearest to 100 mtorr was adopted here), The $\Delta'^{17}O$ profiles for three temperatures do not follow any particular trend (or not parallel to each other), which is a manifestation of the temperature dependent change of the overlapping wave functions in the predissociative process, where the rotational states are also involved.*

Notwithstanding significant uncertainty in the σ-values of $C^{17}O$, we computed (using equation 3 and 4) the $\delta'^{17}O$ values (using available values from literature) through our code and calculated the slope values as a function of wavelengths. The measured $\delta'^{17}O$, $\delta'^{18}O$ and corresponding slope values are compared with the computed values in Figure 5. The measured and computed $\delta'^{18}O$ values are quite different though the overall range of values is nearly the same (Figures 2b and 5). The same is true for the $\delta'^{17}O$ values. Isotopologue specific absorption might be partly responsible for the measured enrichments but we think that the isotope effect in the dissociative steps following the photon absorption, i.e., the predissociative processes significantly modulates the final fractionation.

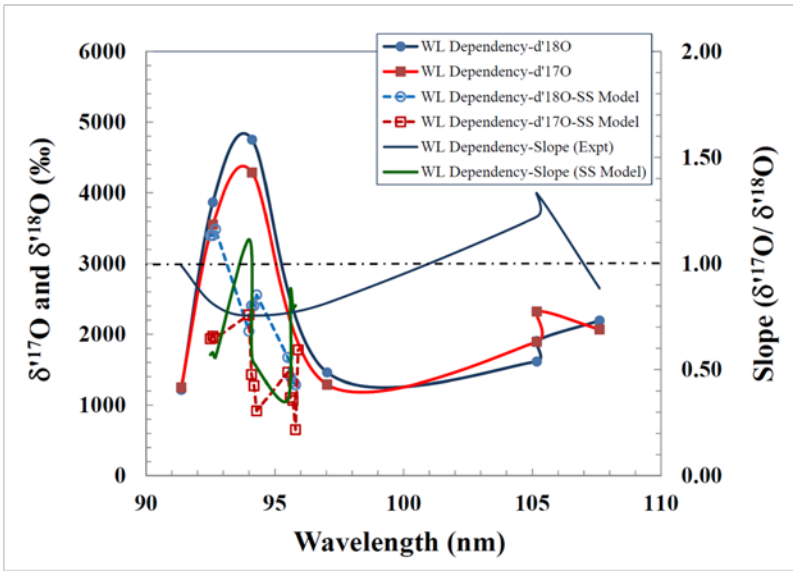

Figure 5. *Wavelength dependent variation in measured and model computed $\delta'^{17}O$ and $\delta'^{18}O$ along with the slope values (right axis).*

The oxygen isotopic fractionation estimate based on isotope self-shielding model depends on the absorption cross-section of the molecule at a specific wavelength and the column density of the gas. Isotope self-shielding should generate isotopically enriched atomic pools of carbon and oxygen. For oxygen, equal dissociation of $C^{17}O$ and $C^{18}O$ [1, 2, 4, 43, 47, 48] in the shielded zone would yield a slope ($\delta'^{17}O$/ $\delta'^{18}O$) value of unity for the product CO_2. Increasing CO column density would eventually shield $C^{18}O$ resulting in more preferential dissociation of $C^{17}O$ compared to $C^{18}O$, yielding slope value greater than unity [43]. The column density versus the slope value (for 105.17 and 107.6 nm) plot (Figure 6) does not depict such a relationship given the fact that the absorption cross-section of 107.6 nm band is ~2.5 times stronger than 105.17 nm band. Figure 6 shows that for 107 nm, with increasing pressure the slope values remain almost the same (within uncertainty, from 0.96 to 0.92). For 105 nm the slope value shows a non-linear trend initially increasing from 0.88 to 1.42, and then decreasing to 1.35 at highest column density. The non-linear trend (Figure 6) could only be explained via isotopologue specific dissociation process. Moreover, a few percent difference in isotopologue specific quantum yield of dissociation would result in several hundred per mil effect in the product as the δ-scales are extremely sensitive. As an illustration, we have run our code by introducing a cross-section damping factor (equivalent to quantum yield). The model result shows that a 10 % reduction of quantum yield of $C^{17}O$ dissociation reduces the $\delta'^{17}O$ value typically by 200 ‰ and that corresponds to slope value reduction from 1.07 to 0.85.

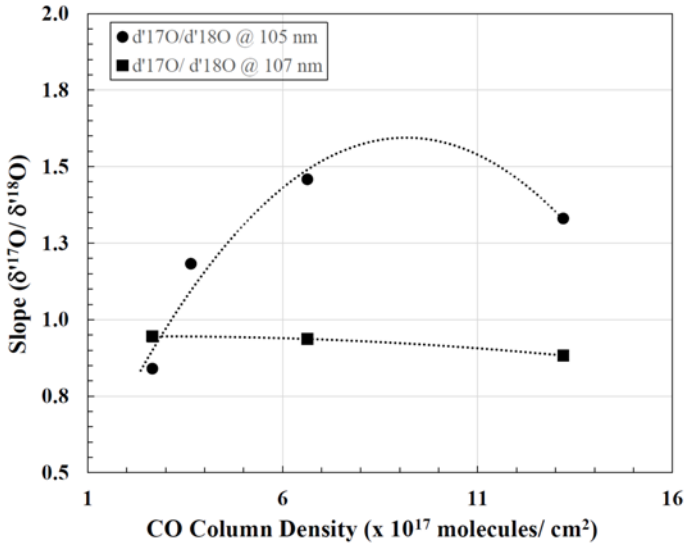

Figure 6. *Column density dependent slope values measured in the experiments at 105 and 107 nm synchrotron bands. There is no systematic increase in slope values for both cases, contrary to that expected for self-shielding mechanism.*

A recent study [43] attempted to explain our previous [11, 17] experimental data using line-by-line CO spectra in a self-shielding model. The article concludes "a lack of published rare isotopologue cross-section data means that significant uncertainties exist for σ and φ (dissociation probability) for $C^{17}O$ and $C^{18}O$. Measurement uncertainties in the oscillator strengths (which characterize the strength of a transition) for CO bands are typically approximately 20–50 % even for $^{12}C^{16}O$. For $^{12}C^{17}O$, no measured oscillator strengths have been published". Thus, the premise of that model computation is inconsistent with the present experiments. Unlike the present experiments, the previous experiments [11, 17] were performed without H_2, but the measured oxygen isotopic compositions are comparable, indicating a negligible role of H_2 in the chemistry in the chamber and product recovery.

6.2. Carbon isotopic fractionations

The product CO_2 is enriched in ^{13}C relative to the starting composition by a few hundred to slightly more than a thousand per mil depending on the wavelength of photodissociation (Figure 1a). Isotope self-shielding should preferentially dissociate ^{13}CO compared to ^{12}CO at greater optical depth in the chamber (along the line of sight of the photons) as explained above [5] and produce a C-atom pool enriched in ^{13}C while keeping the major reservoir of CO essentially unchanged. It is surprising that the measured CO_2 is enriched in ^{13}C. The main path of CO_2 formation inside the chamber is likely through CO + O reaction. In that case, the product CO_2 should not be enriched in ^{13}C, contrary to the measurements. Therefore, in the present experiments (with H_2) some significant chemical reactions must occur which enrich the CO_2 in ^{13}C. Factors such as the ionization of atoms and molecules, the role of H_2 in carbon chemistry may play such a role and should be incorporated in future models. At present, the rate constants of ion-molecular recombination reactions and exchange reactions are mostly unknown. The data can be interpreted in terms of competing reactions (e.g., isotopic fractionation due to photodissociation and ion-molecular exchange reaction) by the following sequence of chemical processes,

$$CO + h\nu \rightarrow C + O \quad (5)$$

$$C + h\nu \rightarrow C^{+} \quad (6)$$

$$^{13}C^{+} + {}^{12}CO \leftrightarrow {}^{12}C^{+} + {}^{13}CO\ (+\ 35\ K) \quad (7)$$

and that should lead to ^{13}C enrichment in CO phase at low temperature [5, 49, 50]. This scheme would ultimately produce ^{13}C enriched CO_2. Exchange reaction between the $^{13}C^{+}$ ion and the ^{12}CO molecule is not the same as an atom-molecule exchange reaction and the forward reaction has zero-point energy advantage of 35K [49]. The rate constants (forward and backward reactions) of the isotope exchange reaction (7) are experimentally determined and verified [50], which show that the rate constant of the forward reaction (5.9×10^{-10} at 80 K)) is 35% faster than the backward reaction. Thus, this exchange mechanism has the potential for enriching CO pool with ^{13}C.

In the present set up the inner diameter of the reaction chamber is 1.25 cm while the synchrotron beam is only of a few micron-size in diameter. Therefore, a micron-size cylindrical zone (a cylinder of a diameter of a few micron and 130 cm in length) is the photoactive zone inside the chamber. The calculated mean free path of the gas molecule in the experimental condition is about 92 μm. Therefore, it is reasonable to consider that the chemical reactions (including isotope exchange reactions) following photodissociation occur in the vicinity of the photoactive zone and the CO gas in the remaining part of the chamber do not participate. This facilitates the local enhancement of ^{13}CO in the photoactive zone that can participate in CO_2 production in the same local region. The factor of 5 lower values of measured ^{13}C enrichments compared to the computed values mentioned before (Figure 2a) might be due to the inefficiency of

this secondary enrichment process to transfer the ^{13}C enrichments to the entire CO_2 pool. Further experimental and modeling effort are underway to understand these results.

7. Implications for Cosmochemistry

CO is the second most abundant molecule in the interstellar medium after hydrogen. In the solar nebula, it is the most abundant oxygen and carbon carrying primordial molecule. Both the elements C and O in CO are enigmatic in terms of accounting for the relevant chemistry in the solar nebula that leads to the formation of planetary solids in the solar system. The isotope ratio of carbon ($^{12}C/^{13}C$) in the solar system is widely accepted to be 89 [51]. The $^{12}C/^{13}C$ ratio at the galactic center is about 62 based on the spectroscopic measurements on CN, CO, and H_2CO [50, 52, 53]. The solar system value is greater than the typical present-day local interstellar medium (LISM) value of ~68 [53]. The Sun formed approximately 1.9 kpc closer to the galactic center than its present location (7.94 kpc), presumably in a region with a lower $^{12}C/^{13}C$ ratio [53]. The difference between this value and the present solar system value of 89 indicates that the solar system must have become either significantly enriched in ^{12}C, or there was a significant depletion of ^{13}C during galactic chemical evolution [54, 55]. Though the average solar system value $^{12}C/^{13}C$ is 89, a significant variation among different primitive solar system bodies is found [50, 56-61] with both depleted and enriched ^{13}C. The lowest $^{12}C/^{13}C$ ratio of 42.5 (i.e., $\delta^{13}C$ = 1100 ‰ rel. to VPDB) was measured in the Murchison carbonaceous chondritic meteorite [61]. A ratio of 45.5 (i.e., $\delta^{13}C$ = 964 ‰) was measured in a cometary grain [58]. The presence of such extreme ^{13}C enrichments within solar system materials might be indicative of photochemical processes in the early solar nebula. Isotopologue specific photodissociation can produce ^{13}C enriched atomic carbon pool as shown in the present experiments. Since carbon has only 2 stable isotopes (^{12}C and ^{13}C), unlike oxygen (three stable isotopes: ^{16}O, ^{17}O and ^{18}O), there is no way of distinguishing between the individual photochemical process, e.g., self-shielding or isotopologue specific predissociation.

With respect to oxygen isotopes, there are two outstanding enigmas present in solar system planetary materials (i) the solar system $^{18}O/^{17}O$ ratio (5.2) is significantly higher than the present-day Inter Stellar Medium value (~ 4) possibly due to enrichment of the protosolar molecular cloud by ^{18}O-rich supernova ejecta before or during solar system formation, and (ii) oxygen isotopes are heterogeneously distributed in the solar system on all distance scales [62]. The most primitive solid objects in the solar system follow a trend line of slope ($\delta'^{17}O/\delta'^{18}O$) unity in oxygen three-isotope space. There is no broad agreement as to the underlying mechanism for this heterogeneity but generally, the photochemical processing was preferred and isotope self-shielding has been suggested as a plausible mechanism. With the help of triple oxygen isotope fractionation variation based on the present experimental results, it is possible to distinguish between the photochemical processes. On one hand, different slope values ($\delta'^{17}O/\delta'^{18}O$) at different wavelengths as measured in the present experiments could be possible through a self-shielding mechanism (via differential isotopologue specific absorption cross section) as well as through isotopologue specific photodissociation. On the other hand, the measured trend in pressure-dependent slope values (Figure 6) is not consistent with self-shielding. Chemical reactions (e.g., $SiO + OH \rightarrow SiO_2 + H$)) or photochemical processes (non-shielding types as shown in the present experiments) can produce slope 1 in oxygen three-isotope space [63], [1, 4, 17, 63, 64]. It is also interesting to note that the variability within the solar system is primarily in the abundance of ^{16}O

whereas, the $^{18}O/^{17}O$ ratio is well constrained (5.2 ± 0.2) [54, 65]. These findings make the photochemical evolution of CO a matter of central importance.

8. Conclusions

New 80K data related to photodissociation of CO support the hypothesis that perturbation dominated state mixing (through overlapping wave functions) dynamics determines which isotopologues preferentially dissociate. They also show that the quantum yields of dissociation are much less than unity. Differential absorption of a photon by the major isotopologue (leading to self-shielding) does contribute towards isotopic discrimination in the experimental photodissociation products, but we propose that the major isotopic modulation occurs by the predissociative process. With lowering of temperatures, the state mixing dynamics change dramatically in localized zones (perturbation and coupling associated with a state) and produces a large difference between fractionations at ambient and low temperatures. This finding confirms that predissociation processes play a big role in determining the isotopic composition of the photodissociation products. The present results are inconsistent with a self-shielding model which was invoked to explain the oxygen isotopic distribution of early solar system objects showing a slope one trend in oxygen three-isotope space. However, both the self-shielding model [1] and the self-shielding based model calculation presented here rely on the isotopologue specific photodissociation cross-section data, which have not been measured with sufficient accuracy (± 10 %) to date to achieve the precision required to define the tight slope of unity measured in the meteorites. Further cross-section data are required to provide a better understanding of the meteorite slope.

Acknowledgment

The work is funded through NASA's Origins, Cosmochemistry, and Emerging Worlds programs. SC and MHT gratefully acknowledge support from NASA. MA is supported by the Director, Office of Science, Office of Basic Energy Sciences, of the U.S. Department of Energy under Contract No. DE-AC02-05CH11231, through the Gas Phase Chemical Physics Program, Chemical Sciences Division. BR and the ALS are also supported under Contract No. DE-AC02-05CH11231.

References

[1] J.R. Lyons, E.D. Young, CO self-shielding as the origin of oxygen isotope anomalies in the early solar nebula, Nature 435 (2005) 317-320.
[2] R. Visser, E. van Dishoeck, F., J. Black, H., The photodissociation and chemistry of CO isotopologues: applications to interstellar clouds and circumstellar disks, A&A 503 (2009) 323-343.
[3] R.N. Clayton, L. Grossman, T.K. Mayeda, A Component of Primitive Nuclear Composition in Carbonaceous Meteorites, Science 182 (1973) 485-488.
[4] H. Yurimoto, K. Kuramoto, Molecular Cloud Origin for the Oxygen Isotope Heterogeneity in the Solar System, Science 305 (2004) 1763-1766.
[5] E.F. vanDishoeck, J.H. Black, The photodissociation and chemistry of interstellar CO, Astrophysical Journal 334 (1988) 32.
[6] H. Lefebvre-Brion, R.W. Field, The Spectra and Dynamics of Diatomic Molecules, 2nd ed., Elsevier Academic Press2004.
[7] H. Lefebvre-Brion, B.R. Lewis, Comparison between predissociation mechanisms in two isoelectronic molecules: CO and N2, Molecular Physics 105 (2007) 1625-1630.
[8] K.S.E. Eikema, W. Hogervorst, W. Ubachs, Predissociation rates in carbon monoxide: dependence on rotational state, parity and isotope, Chemical Physics 181 (1994) 217-245.
[9] K.S.E. Eikema, W. Hogervorst, W. Ubachs, On the Determination of a Heterogeneous vs a Homogeneous Perturbation in the Spectrum of a Diatomic Molecule: The K1[Sigma]+, v = 0 state of 13C18O, Journal of Molecular Spectroscopy 163 (1994) 19-26.
[10] H. Lefebvre-Brion, R. Colin, Anomalous isotope effects in indirect predissociations : An example in the spectrum of BeH, Journal of Molecular Spectroscopy 65 (1977) 33-45.

[11] S. Chakraborty, R.D. Davis, M. Ahmed, T.L. Jackson, M.H. Thiemens, Oxygen isotope fractionation in the vacuum ultraviolet photodissociation of carbon monoxide: Wavelength, pressure, and temperature dependency, The Journal of Chemical Physics 137 (2012) 024309-024312.
[12] O. Atabek, R. Lefebvre, A. Requena, Semiclassical model for accidental predissociation in diatomic molecules, Journal of Molecular Spectroscopy 82 (1980) 364-378.
[13] A.J. Lorquet, J.C. Lorquet, Isotopic effects in accidental predissociation. The case of the C2[Sigma]+u state of N+2, Chemical Physics Letters 26 (1974) 138-143.
[14] S.A. Ndengué, F. Gatti, R. Schinke, H.-D. Meyer, R. Jost, Absorption Cross Section of Ozone Isotopologues Calculated with the Multiconfiguration Time-Dependent Hartree (MCTDH) Method: I. The Hartley and Huggins Bands, The Journal of Physical Chemistry A 114 (2010) 9855-9863.
[15] S.A. Ndengué, R. Schinke, F. Gatti, H.-D. Meyer, R. Jost, Ozone Photodissociation: Isotopic and Electronic Branching Ratios for Symmetric and Asymmetric Isotopologues, The Journal of Physical Chemistry A 116 (2012) 12271-12279.
[16] C.E. Miller, R.M. Onorato, M.C. Liang, Y.L. Yung, Extraordinary isotopic fractionation in ozone photolysis, Geophysical Research Letters 32 (2005).
[17] S. Chakraborty, M. Ahmed, T.L. Jackson, M.H. Thiemens, Experimental test of self-shielding in vacuum ultraviolet photodissociation of CO, Science 321 (2008) 1328-1331.
[18] S. Chakraborty, M. Ahmed, T.L. Jackson, M.H. Thiemens, Response to Comments on "Experimental Test of Self-Shielding in Vacuum Ultraviolet Photodissociation of CO", Science 324 (2009) 4.
[19] S. Chakraborty, T.L. Jackson, M. Ahmed, M.H. Thiemens, Sulfur isotopic fractionation in vacuum UV photodissociation of hydrogen sulfide and its potential relevance to meteorite analysis, Proceedings of the National Academy of Sciences 110 (2013) 17650-17655.
[20] S. Chakraborty, B.H. Muskatel, T.L. Jackson, M. Ahmed, R.D. Levine, M.H. Thiemens, Massive isotopic effect in vacuum UV photodissociation of N2 and implications for meteorite data, Proceedings of the National Academy of Sciences 111 (2014) 14704-14709.
[21] S. Chakraborty, T.L. Jackson, B. Rude, M. Ahmed, M.H. Thiemens, Nitrogen isotopic fractionations in the low temperature (80 K) vacuum ultraviolet photodissociation of N2, The Journal of Chemical Physics 145 (2016) 114302.
[22] A.N. Heays, R. Visser, R. Gredel, W. Ubachs, B.R. Lewis, S.T. Gibson, E.F. van Dishoeck, Isotope selective photodissociation of N2 by the interstellar radiation field and cosmic rays, A&A 562 (2014) A61.
[23] B.H. Muskatel, F. Remacle, M.H. Thiemens, R.D. Levine, On the strong and selective isotope effect in the UV excitation of N2 with implications toward the nebula and Martian atmosphere, Proceedings of the National Academy of Sciences 108 (2011) 6020.
[24] J.L. Lemaire, M. Eidelsberg, A.N. Heays, L. Gavilan, S.R. Federman, G. Stark, J.R. Lyons, N.d. Oliveira, D. Joyeux, High-resolution spectroscopy of the ##IMG## [http://ej.iop.org/images/0953-4075/49/15/154001/toc_jpbaa29ecieqn1.gif] {${A}^{1}{\rm{\Pi }}(v^{\prime} =0\mbox{--}10)\mbox{--}{X}^{1}{{\rm{\Sigma }}}^{+}(v^{\prime\prime} =0)$} bands in 13 C 18 O: term values, ro-vibrational oscillator strengths and Hönl–London corrections, Journal of Physics B: Atomic, Molecular and Optical Physics 49 (2016) 154001.
[25] A.N. Heays, M. Eidelsberg, G. Stark, J.L. Lemaire, L. Gavilan, S.R. Federman, B.R. Lewis, J.R. Lyons, N. de Oliveira, D. Joyeux, Observation of a new electronic state of CO perturbing WΠ1(v=1), The Journal of Chemical Physics 141 (2014) 144311.
[26] G. Stark, A.N. Heays, J.R. Lyons, P.L. Smith, M. Eidelsberg, S.R. Federman, J.L. Lemaire, L. Gavilan, N.d. Oliveira, D. Joyeux, L. Nahon, High-Resolution Oscillator Strength Measurements of the v' = 0,1 Bands of the B-X, C-X, and E-X Systems in Five Isotopologues of Carbon Monoxide, The Astrophysical Journal 788 (2014) 67.
[27] M. Eidelsberg, J.L. Lemaire, S.R. Federman, G. Stark, A.N. Heays, L. Gavilan, J.R. Lyons, P.L. Smith, N. de Oliveira, D. Joyeux, High-resolution study of oscillator strengths and predissociation rates for 13C16O and 12C18O, A&A 566 (2014) A96.
[28] H. Lefebvre-Brion, M. Eidelsberg, New experimental study and theoretical model of the extreme UV absorption spectrum of CO isotopologs, Journal of Molecular Spectroscopy 271 (2012) 59-65.
[29] M. Eidelsberg, J.L. Lemaire, S.R. Federman, G. Stark, A.N. Heays, Y. Sheffer, L. Gavilan, J.-H. Fillion, F. Rostas, J.R. Lyons, P.L. Smith, N. de Oliveira, D. Joyeux, M. Roudjane, L. Nahon, High-resolution study of oscillator strengths and predissociation rates for 12C16O, A&A 543 (2012) A69.
[30] S. Warin, J.J. Benayoun, Y.P. Viala, Photodissociation and rotational excitation of interstellar CO, Astronomy and Astrophysics 308 (1996) 29.
[31] Y. Sheffer, et al., High-Resolution Measurements of Intersystem Bands of Carbon Monoxide toward X Persei, The Astrophysical Journal Letters 572 (2002) L95.

[32] C. Letzelter, M. Eidelsberg, F. Rostas, J. Breton, B. Thieblemont, Photoabsorption and photodissociation cross sections of CO between 88.5 and 115 nm, Chemical Physics 114 (1987) 16.
[33] M. Eidelsberg, J.J. Benayoun, Y. Viala, F. Rostas, P.L. Smith, K. Yoshino, G. Stark, C.A. Shettle, Recalibration of the absorption/photodissociation spectra of CO and its isotopes between 91 and 115 NM, Astronomy and Astrophysics 265 (1992) 839-842.
[34] M. Eidelsberg, J.L. Lemaire, J.H. Fillion, F. Rostas, S.R. Federman, Y. Sheffer, Oscillator strengths for transitions to Rydberg levels in $\mathsf{^{12}}$C$\mathsf{^{16}}$O, $\mathsf{^{13}}$C$\mathsf{^{16}}$O and $\mathsf{^{13}}$C$\mathsf{^{18}}$O between 967 and 972 Å, A&A 424 (2004) 355-361.
[35] J.D. Simmons, S.G. Tilford, Evidence for an accidental predissociation of CO, Journal of Molecular Spectroscopy 49 (1974) 167-168.
[36] J. Baker, F. Launay, The k3[Pi] Valence State of CO, Journal of Molecular Spectroscopy 165 (1994) 75-87.
[37] W. Ubachs, I. Velchev, P. Cacciani, Predissociation in the E [sup 1] Pi, v = 1 state of the six natural isotopomers of CO, The Journal of Chemical Physics 113 (2000) 547-560.
[38] J. Baker, J.L. Lemaire, S. Couris, A. Vient, D. Malmasson, F. Rostas, A 2+1 REMPI study of the E-X transition in CO. Indirect predissociations in the E 1[Pi] state, Chemical Physics 178 (1993) 569-579.
[39] P. Cacciani, W. Hogervorst, W. Ubachs, Accidental predissociation phenomena in the E 1 Pi, v=0 and v=1 states of 12C16O and 13C16O, The Journal of Chemical Physics 102 (1995) 8308-8320.
[40] M. Eidelsberg, F. Rostas, Spectroscopic, absorption and photodissociation data for CO and isotopic species between 91 and 115 nm, A&A 235 (1990).
[41] P. Cacciani, W. Ubachs, High resolution study of Q-branches in the E1[Pi]-X1[Sigma]+ (0,0) band of 12C16O, 13C16O, and 13C18O, Journal of Molecular Spectroscopy 225 (2004) 62-65.
[42] H. Craig, Isotopic standards for carbon and oxygen and correction factors for mass-spectrometric analysis of carbon dioxide, Geochimica et Cosmochimica Acta 12 (1957) 133-149.
[43] J.R. Lyons, Photodissociation of CO isotopologues: Models of laboratory experiments and implications for the solar nebula, Meteoritics & Planetary Science 49 (2014) 373-393.
[44] S. Chakraborty, B. Rude, M. Ahmed, M.H. Thiemens, Data from: Carbon and oxygen isotopic fractionation measurements in the low temperature VUV photodissociation products of carbon monoxide: https://doi.org/10.6075/J0V9868D, 2018.
[45] S.K. Bhattacharya, M.H. Thiemens, NEW EVIDENCE FOR SYMMETRY DEPENDENT ISOTOPE EFFECTS - O+CO REACTION, Zeitschrift Fur Naturforschung Section a-a Journal of Physical Sciences 44 (1989) 435-444.
[46] J.P. Bouanich, On the temperature dependence of self-broadening in the first overtone band of CO, Journal of Quantitative Spectroscopy and Radiative Transfer 31 (1984) 561-567.
[47] J.R. Lyons, E.A. Bergin, F.J. Ciesla, A.M. Davis, S.J. Desch, K. Hashizume, J.E. Lee, Timescales for the evolution of oxygen isotope compositions in the solar nebula, Geochimica Et Cosmochimica Acta 73 (2009) 4998-5017.
[48] E.D. Young, K. Kuramoto, R.A. Marcus, H. Yurimoto, S.B. Jacobsen, Mass-independent oxygen isotope variation in the solar nebula, in: G.J. MacPherson, D.W. Mittlefehldt, J.H. Jones, S.B. Simon (Eds.), 2008, pp. 187-218.
[49] W.D. Watson, V.G. Anicich, J. Huntress, W. T., Measurement and significance of the equilibrium reaction C-13/+/ + /C-12/O yields C-12/+/ + /C-13/O for alteration of the C-13/C-12 ratio in interstellar molecules, Astrophys. J. Lett. 205 (1976) L165-L168.
[50] P.M. Woods, Carbon isotope measurements in the Solar System, ArXiv e-prints, 2009.
[51] E. Anders, N. Grevesse, Abundances of the elements: Meteoritic and solar, Geochimica Et Cosmochimica Acta 53 (1989) 197-214.
[52] T.L. Wilson, R.T. Rood, Abundances in the Interstellar Medium, Annual Review of Astronomy and Astrophysics 32 (1994) 191-226.
[53] S.N. Milam, C. Savage, M.A. Brewster, L.M. Ziurys, S. Wyckoff, The 12C/13C Isotope Gradient Derived from Millimeter Transitions of CN: The Case for Galactic Chemical Evolution, The Astrophysical Journal 634 (2005) 1126.
[54] L.R. Nittler, E. Gaidos, Galactic chemical evolution and the oxygen isotopic composition of the solar system, Meteoritics & Planetary Science 47 (2012) 2031-2048.
[55] L.S. Rachel, M.P. Klaus, D.Y. Edward, R.M. Mark, Heterogeneity in 12CO/13CO Abundance Ratios toward Solar-type Young Stellar Objects, The Astrophysical Journal 813 (2015) 120.
[56] M.M. Grady, I.P. Wright, P.K. Swart, C.T. Pillinger, The carbon and oxygen isotopic composition of meteoritic carbonates, Geochimica et Cosmochimica Acta 52 (1988) 2855-2866.
[57] M.H. Engel, S.A. Macko, J.A. Silfer, Carbon isotope composition of individual amino acids in the Murchison meteorite, Nature 348 (1990) 47-49.

[58] K.D. McKeegan, J. Aléon, J. Bradley, D. Brownlee, H. Busemann, A. Butterworth, M. Chaussidon, S. Fallon, C. Floss, J. Gilmour, M. Gounelle, G. Graham, Y. Guan, P.R. Heck, P. Hoppe, I.D. Hutcheon, J. Huth, H. Ishii, M. Ito, S.B. Jacobsen, A. Kearsley, L.A. Leshin, M.-C. Liu, I. Lyon, K. Marhas, B. Marty, G. Matrajt, A. Meibom, S. Messenger, S. Mostefaoui, S. Mukhopadhyay, K. Nakamura-Messenger, L. Nittler, R. Palma, R.O. Pepin, D.A. Papanastassiou, F. Robert, D. Schlutter, C.J. Snead, F.J. Stadermann, R. Stroud, P. Tsou, A. Westphal, E.D. Young, K. Ziegler, L. Zimmermann, E. Zinner, Isotopic Compositions of Cometary Matter Returned by Stardust, Science 314 (2006) 1724-1728.
[59] C.M.O.D. Alexander, S.S. Russell, J.W. Arden, R.D. Ash, M.M. Grady, C.T. Pillinger, The origin of chondritic macromolecular organic matter: A carbon and nitrogen isotope study, Meteoritics & Planetary Science 33 (1998) 603-622.
[60] J.F. Kerridge, Carbon, hydrogen and nitrogen in carbonaceous chondrites: Abundances and isotopic compositions in bulk samples, Geochimica et Cosmochimica Acta 49 (1985) 1707-1714.
[61] P.K. SWART, M.M. GRADY, C.T. PILLINGER, R.S. LEWIS, E. ANDERS, Interstellar Carbon in Meteorites, Science 220 (1983) 406-410.
[62] M.H. Thiemens, History and Applications of Mass-Independent Isotope Effects, Annual Review of Earth and Planetary Sciences 34 (2006) 217-262.
[63] S. Chakraborty, P. Yanchulova, M.H. Thiemens, Mass-Independent Oxygen Isotopic Partitioning During Gas-Phase SiO2 Formation, Science 342 (2013) 463-466.
[64] Y. Kimura, J.A. Nuth, S. Chakpaborty, M.H. Thiemens, Non-mass-dependent oxygen isotopic fractionation in smokes produced in an electrical discharge, Meteoritics & Planetary Science 42 (2007) 1429-1439.
[65] D.Y. Edward, G. Matthieu, L.S. Rachel, R.M. Mark, M.P. Klaus, Astronomical Oxygen Isotopic Evidence for Supernova Enrichment of the Solar System Birth Environment by Propagating Star Formation, The Astrophysical Journal 729 (2011) 43.